MATEC Web of Conferences **14**, 09001 (2014)
DOI: 10.1051/matecconf/20141409001

The effect of Ru on precipitation of topologically close packed phases in Re – containing Ni base superalloys: Quantitative FIB-SEM investigation and 3D image modeling

Kamil Matuszewski[a], Ralf Rettig, and Robert F. Singer

Institute of Science and Technology of Metals WTM, Department of Materials Science and Engineering, University of Erlangen-Nuremberg FAU, Martensstr. 5, 91058 Erlangen, Germany

Abstract. A new approach to clarify the ruthenium effect on the precipitation of topologically close packed (TCP) phases is described in the paper. It is based on focused ion beam – scanning electron microscopy (FIB – SEM) dual beam methodology as well as three-dimensional imaging. The high-temperature capabilities of nickel base superalloys can be improved by alloying with refractory elements. With excessive refractory element content or excessive exposure to high temperature, brittle TCP phases precipitate resulting in a drop of strength. The undesirable phase transformation can be suppressed by addition of ruthenium. Although the effect is well known, its real mechanism remains open. In the present paper, the volume fraction and particle density, as well as the exact three-dimensional morphology of TCP phases as measured by FIB-SEM will be presented. The effect of ruthenium content and time of exposure is studied quantitatively. The results show that increased Ru additions slow down all stages of phase transformation and also reduce the equilibrium TCP volume fraction. The Ru effect might be due to either reduced driving force for precipitation or reduced interfacial energy.

1. Introduction

Rhenium, with its very low diffusion coefficient [1,2] in a γ-matrix phase, brings a significant improvement in high temperature capability of nickel base superalloys. Heckl et al. reported that the temperature capability increases by 87 K when Re content is increased from 1 to 2 at.% [3]. However, beside the beneficial effect, Re causes also disadvantages like strong segregation of itself to the dendrite core during solidification process [4,5]. Such segregation cannot be fully reversed even by expensive long-term heat-treatments. Moreover, during long-term high-temperature exposure, Re will provoke phase instability, i.e. precipitation of deleterious topologically close packed (TCP) phases [6–11].

TCP phases are formed mostly from refractory elements. They are very brittle and, while growing, deplete the matrix from strengtheners, decreasing stress rupture properties [7,11]. In addition, with their complex morphology [12] they eventually lead to decreased fatigue life-time [11]. Precipitation of TCP phases can be slowed down or even suppressed by the addition of ruthenium to the alloy [7,13]. Because of the high cost of both elements, it is of particular importance to optimize their content in the alloy and to understand the exact way they influence precipitation of TCP phases. Since the so called "reverse partitioning" effect [14,15] cannot be the only mechanism [1,7,13,14] responsible for the Ru influence on the TCP phase precipitation, the question of the exact nature of this phenomenon remains open.

In the present paper we follow a new approach to clarify the Ru influence on the precipitation of TCP phases. The conventional 2D sectioning and quantitative measurements in SEM is accompanied by the new 3D image analysis based on Focused Ion Beam (FIB) tomography. The results obtained allow for the quantitative description of phase transformation in the investigated alloys. It will be verified whether precipitation of TCP phases follows the Johnson-Mehl-Avrami (JMA) [16,17] equation describing phase transformations by nucleation and growth. Moreover, the results are complemented by simulations with respect to the thermodynamics of the alloys.

2. Experimental procedures

2.1. Material

Materials used to investigate the mechanism of Ru influence on TCP phase precipitation are experimental Ni-based superalloys of the 3rd and 4th generations. The detailed chemical compositions are given in Table 1. The alloys contain 2 at. % of Re, while Ru content assumes values of 0, 1 and 2 at.%, respectively for Astra 1–20, −21 and −22. Ruthenium is added to the alloy at the expense of Ni, i.e. all other elements are kept constant.

Materials were produced in a vacuum arc furnace and subsequently converted into columnar grained rods in a Bridgman vacuum induction melting furnace.

[a] Corresponding author: kamil.matuszewski@ww.uni-erlangen.de

Table 1. Chemical composition of investigated alloys (at.%).

	Astra 1-20	Astra 1-21	Astra 1-22
Al	13.5	13.5	13.5
Co	9.0	9.0	9.0
Cr	6.0	6.0	6.0
Mo	0.6	0.6	0.6
Re	2.0	2.0	2.0
Ru	0.0	1.0	2.0
Ta	2.2	2.2	2.2
W	2.0	2.0	2.0
Ni	bal.	bal.	bal.

Table 2. Heat-treatment process parameters.

Step	Heating rate [K/min]	Temperature [° C]	Holding time [h]	Cooling
Solutioning	4	1340	16	In air
1st annealing	4	1140	2	In air
2nd annealing	4	870	24	In air

More specifically, clusters of three cylindrical rods were cast, 180 mm in length and 12 mm in diameter. A withdrawal rate of 9 mm/min resulted in a directionally solidified (DS) structure with a primary dendrite arm (PDA) spacing of 180 μm.

The heat-treatment applied after casting consisted of three steps: homogenisation at 1340 °C for 16 h to decrease the segregation of refractory elements and two aging steps to precipitate the γ' phase and stabilize its morphology. The detailed information about heat-treatment process is given in Table 2. Each step of heat-treatment was conducted under Ar atmosphere. Samples were cooled down in static air.

Heat-treated samples were cut into pieces of 10 mm in height and 12 mm in diameter to be able to apply different subsequent annealing conditions. The annealing process was conducted under Ar atmosphere. This work is focused on the results obtained at 1050 °C and times from 5 to 2000 h. The intervals were adjusted during heat-treatment to be able to fully describe precipitation characteristics which resulted in the following times: 5, 10, 15, 25, 50, 100, 500, 1000, 1500, 2000 h.

The annealed samples were prepared for microscopic observation via metallographic techniques, i.e. gradual grinding and polishing.

2.2. Microscopic observation

The micrographs were obtained on a Helios NanoLab 600i Focused Ion Beam – Scanning Electron Microscope (FIB-SEM) instrument. Two dimensional cross-sections were collected with the use of concentric backscattered electron detector (CBS) with an in-lens mode what resulted in ultra-high resolution images. Samples were observed on (001) planes of γ/γ' phases.

The real three-dimensional (3D) morphology of TCP phases was obtained by the automated sectioning of the material. The Ga ion gun with a beam current of 0.79 nA allowed for obtaining the single slice thickness of 20 nm. 400 slices with the width and height of 10 μm resulted in a total scanned volume of 800 μm^3 within a reasonable time of ion thinning.

2.3. Image processing and quantitative analysis

The reconstruction of the volume and calculations were made with the use of FEI's Visualization Sciences Group AvizoFire software. The volume of interest was reconstructed by adding slice to slice. When necessary the aligning algorithm was applied to bring all of the slices to the same position and correct the drifting problem. Image processing algorithms, like thresholding, were applied to extract TCP phases only from the γ/γ'/TCP microstructure. Extracted phases were then analysed to obtain the real three-dimensional information about the precipitation progress, i.e. morphology and volume fraction. Application of the processing algorithms resulted in a decrease of the analyzed volume.

Area- and volume- fraction for 2D and 3D measurements, respectively, were calculated by dividing the number of pixels/voxels corresponding to TCP phases by the total number of scanned pixels/voxels. For 2D microanalysis, measurements were done on 15 to 20 micrographs for each sample. 3D measurements were done in the full prepared volume, i.e. ~400 μm^3.

2.4. Thermodynamic calculations

Thermodynamic properties were calculated using the CALPHAD (Calculation of Phase Diagrams) method with commercially available software ThermoCalc 3.1 with the thermodynamic database TTNi8.

The compositional data used for thermodynamic calculation were collected with the use of the Electron Probe Microanalysis (EPMA, JXA-8100, JEOL). The mapping measurements were done with the step size of 2.5 μm and dwell time of 200 ms, covering the analyzed area of 0.4 mm^2. A 20 kV acceleration voltage was applied.

3. Results

3.1. Microstructure in 2D

3.1.1. Early stages and equilibrium stages of TCP phase precipitation

The microstructures of the investigated nickel base superalloys are presented in Figs. 1 and 2. Micrographs are taken on (100) planes transverse to the solidification direction.

In Fig. 1 Ru content increases from the top to the bottom and time increases from the left to the right. Ru influence on the early stages of precipitation, i.e. 5 hrs at 1050 °C is shown in Figs. 1a, c, e. It is apparent that 5 hrs of annealing is long enough for the precipitation of TCP phases to start. After 5 hrs of annealing the dominating phases are cuboidal γ'-particles embedded in γ matrix. TCP phases occur as very thin (~30 nm) needles aligned to γ particle cuboidal faces by the angle of 45°. There are also somewhat thicker needles, but 2D observation, even in ultra high resolution mode, is not sufficient to distinguish if these belong to the same type of TCP phases. In fact the

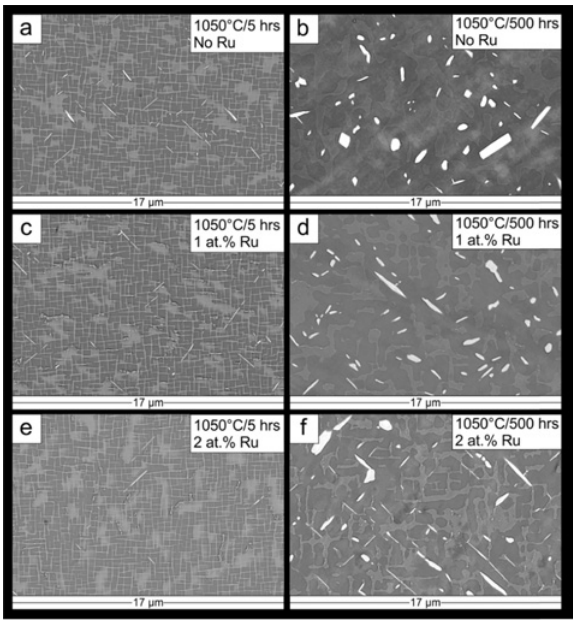

Figure 1. The microstructure of the investigated alloys (Astra 1-20, Astra 1-21, Astra 1-22) observed on (100) planes. The content of Ru changes from the top to the bottom: a,b) no Ru, c,d) 1 at.% Ru, e,f) 2 at.% Ru. The annealing was conducted at 1050 °C for a,c,e) 5 hrs and b,d,f) 500 hrs. TCP phases are visible as white particles due to the high refractory element composition. γ'-phase is imaged in dark- and γ-phase in light-grey colour.

thin needles are supposed to be particles of planar sigma phase which precipitate on $\{111\}$ planes [6,8,12].

After 500 hrs of annealing the alloy achieves equilibrium as is born out by the fact that further annealing till 2000 hrs does not produce any changes. The microstructure in equilibrium is drastically different from the initial one. Generally it is observed that in equilibrium stage there is almost none of the initial γ/γ' cuboidal microstructure. TCP phases exhibit more 'bulky' morphology and the new matrix is γ'-phase. It exhibits an irregular morphology forming continuous envelopes around TCP particles. The γ-phase is observed in the shape of irregular islands (coloured light-grey in Fig. 6b, d, f). The influence of Ru on the equilibrium stage is shown in Figs. 1b, d and f. The addition of ruthenium does not seem to affect the morphology of TCP phases, but it seems that the area fraction is reduced when Ru is present. For the alloys containing 1 or 2 at.% of Ru, very small regions with the initial cuboidal γ/γ' microstructure and plate-like TCP phases can still be observed.

3.1.2. Intermediate stages of TCP phase precipitation: precipitation sequence

Microstructure in Fig. 2 represents the alloy without Ru (Astra 1-20) after 50 hrs of annealing at 1050 °C. The initial γ/γ' microstructure can be observed with some TCP phases precipitated. The main form of TCP phases is a plate-like shape, which appears as needle on cross-sections. More bulky shaped particles are also present within the microstructure. It seems that the bulky phases grow at the expense of plate-like sigma phase, i.e. in

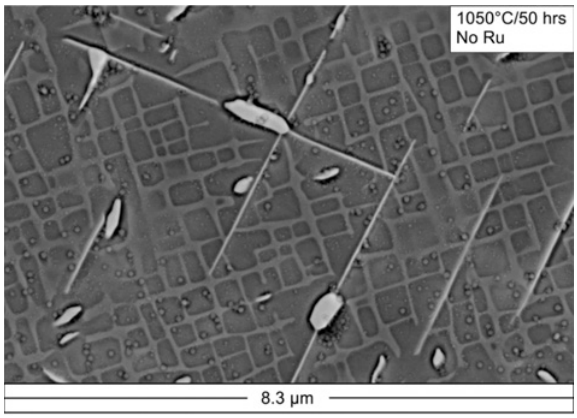

Figure 2. The microstructure of the alloy Astra 1-20 (no Ru) after 50 hrs of annealing at 1050 °C. The plates of sigma phase start to give way for growth of secondary phases. The critical points of new phases growth seem to be the nodes, where two existing phases cross.

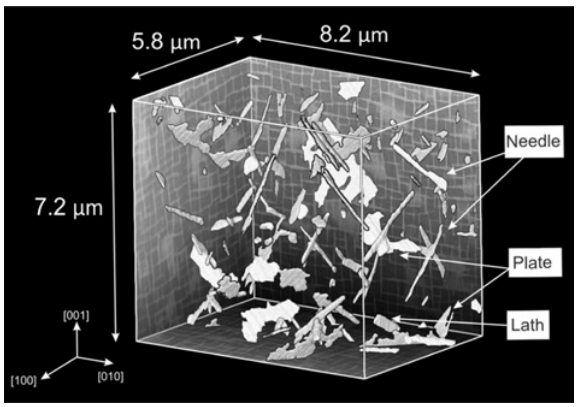

Figure 3. 3D microstructure of the alloy Astra 1-20 after 5 hrs of annealing at 1050 °C. The complex morphology of TCP plates is apparent. One can distinguish at least two types of precipitates: dominating are plates but some needle- or lath-like particles are also observed.

the sense of a precipitation sequence. This is well in accordance with postulates of Darolia [6] that sigma is the first phase to form from the initial microstructure and that sigma is metastable. With the time of annealing it dissolves giving way to another secondary TCP phase. This assumption is confirmed by the numerical simulations of Rettig [18].

3.2. Microstructure in 3D

The three-dimensional morphology of TCP phases is presented in Figs. 3 and 4 for the initial and equilibrium stage, respectively. The microstructures belong to the alloy Astra 1-20 without addition of Ru.

In the initial stage, it is observed that most of the thin needles visible on 2D cross-sections are in fact plates, most likely being the tetragonal sigma phase. They precipitate on $\{111\}$ planes and have quite complex morphology. In addition there are some TCP precipitates exhibiting needle-like or lath-like shapes rather than plate-like. However, the dominating phase is clearly the plate-like one. The complex morphology of plate-like sigma

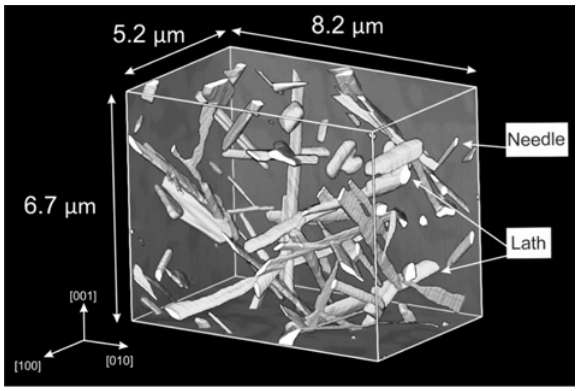

Figure 4. 3D microstructure of the alloy Astra 1-20 after 500 hrs of annealing at 1050 °C. TCP phases exhibit complex morphology, mostly lath-like, but some needle-like particles are also observed. Plates of σ-phase are not observed in equilibrium stage of this alloy.

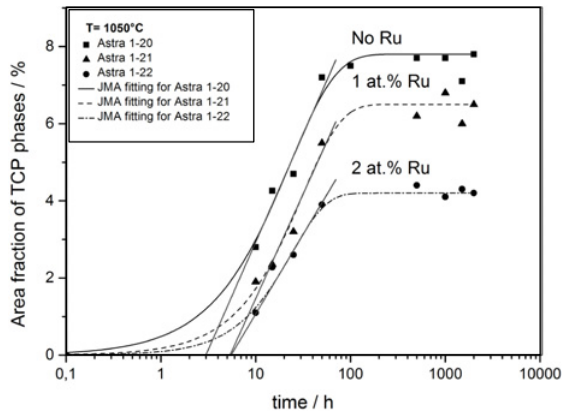

Figure 5. Area fraction of the TCP phase as a function of time for the alloys with different content of Ru. Symbols represent the data obtained experimentally in 2D observation. The curves are obtained via JMA fitting. The straight lines (tangents) determine graphically the initial rapid growth rate and incubation time.

phase is the result of its growth mechanism and interaction with other particles as described in [12].

The 3D morphology of equilibrium stage is presented in Fig. 4. The main difference, in comparison to the initial stage, is the absence of cuboidal γ/γ' microstructure and plate-like TCP particles. TCP phases occur mostly in shape of laths. Their length ranges from just a few to tens of micrometers. Many of investigated particles are cut by the faces of the box of observation, i.e. the dimensions are larger than on first appearance. Needle-like particles are also observed in this stadium, but their content is low.

3.3. Quantitative phase transformation analysis – Johnson-Mehl-Avrami (JMA) equation

3.3.1. Area and volume fraction of TCP phases

The quantitative description of TCP phase precipitation at 1050 °C is given in Fig. 5. The results presented show the influence of Ru and time. Experimental data is plotted as symbols and fitted non-linear with a JMA function [17].

$$y(t) = 1 - \exp(-k \cdot t^{n}). \quad (1)$$

Table 3. Parameters k and n derived from JMA equation.

Material	k	n
Astra 1-20	0.064	0.88
Astra 1-21	0.028	1.05
Astra 1-22	0.022	1.19

The parameters k and n depend on the nucleation and growth processes [17]. Their values were experimentally obtained by the double logarithm operation on JMA equation. For this procedure, it was assumed that equilibrium content of TCP phases refer to 100% of transformation.

$$\ln[\ln(1/1 - y(t))] = n \cdot \ln t + \ln\ k. \quad (2)$$

The obtained values are given in Table 3.

The detailed analysis of the precipitation process is given in the following subsections.

It is obvious from Fig. 5 that precipitation of TCP phases can be described by the JMA equation. This means that the precipitation proceeds in three stages. In the first stage, called incubation, nucleation occurs and speed of transformation is low. The second stage is characterized by steep concentration gradients and rapid growth of precipitates. In the third stage diffusion fields begin to overlap, growth slows down and the equilibrium content of precipitates is reached eventually.

The Ru influence on the TCP phase precipitation is also evident from Fig. 5. For all times investigated, the area fraction of TCP phases decreases with increasing content of Ru. The equilibrium area fraction falls from around 8.0% for no Ru to 6.5% for the addition of 1 at.% Ru and 4.3% for 2 at.% of Ru.

3.3.2. Growth rate

Another quantity which characterizes the precipitation process is the growth rate. As indicated by the initial rapid growth rate (tangents in Fig. 5) the highest rate is observed when no Ru is present in the alloy. With the addition of Ru the growth rate decreases.

3.3.3. Incubation time

The first stage of nucleation and slow transformation, i.e. incubation stage is also influenced by Ru. Incubation time is graphically indicated by the point where the tangent of the rapid growth slope intersects the time axis. Analysing the graph in Fig. 5 it is evident that the shortest incubation time is achieved for the alloy without Ru. When Ru is added the incubation time increases. Although the effect is not so evident between the alloys containing 1 and 2 at.% of Ru, one should mention that the in-house investigations at different temperatures (to be published separately) seem to indicate the increase in incubation time with the addition of Ru.

3.3.4. Nuclei density

Nuclei density is the next very important factor indicating Ru influence on the precipitation of TCP phases. It is given

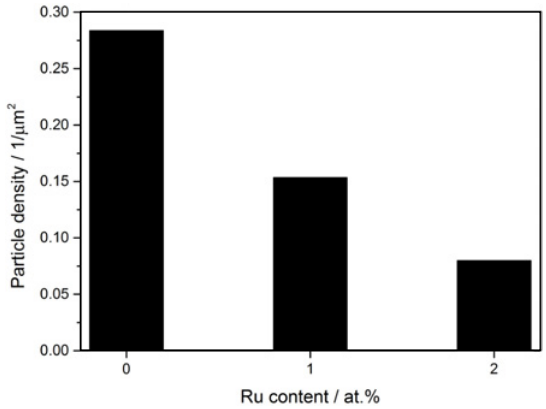

Figure 6. The particle density of TCP phases after 5 hrs at 1050 °C as a function of Ru content. A strong decrease in the particle density is observed when Ru is added to the material.

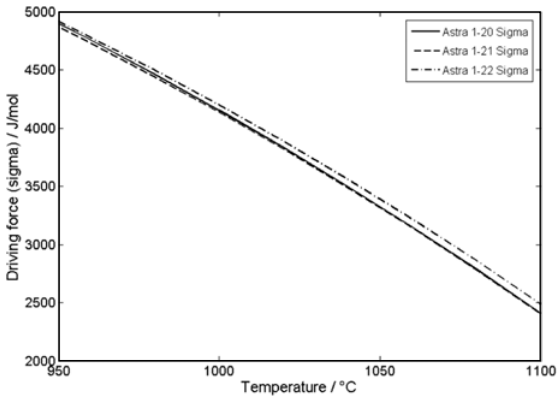

Figure 7. The driving force for precipitation of sigma phase plotted as a function of temperature for alloys with different Ru contents. The calculations were conducted with the use of ThermoCalc 3.1 and TTNi8 database.

by the particle density (number of particles per area) in the early stage of precipitation (5 hrs at 1050 °C) and presented in the form of a bar graph in Fig. 6. The length of analyzed particles was in the range from 0.1 to 3.5 μm.

Quantitative measurements plotted in Fig. 6 show that there is a strong influence of Ru on the particle density. The highest particle density is measured for the alloy without Ru. It decreases significantly, with the factor of 1.8 and 3.6, with the addition of 1 and 2 at.% of Ru, respectively.

3.4. Thermodynamic calculations

The driving force for precipitation of sigma phase in investigated alloys is presented in Fig. 7. Regarding to the calculations it is evident that the driving force decreases with the temperature increase.

An effect of Ru on the driving force is not evident. The values are on the same level and always within the range of error. Regarding to the calculation it seems that Ru does not have any or very little effect on the driving force of the σ phase precipitation. A similar behaviour is observed when the calculations are conducted for the other TCP phases like P or μ.

4. Discussion

4.1. Overall phase transformation

After standard heat-treatment the microstructure consists of cuboidal precipitates of γ'-phase embedded within γ matrix phase. After a certain time, nuclei of TCP phases are formed, which grow in the shape of very thin planar sheets. Such planar morphology (Figs. 1a, c, e, 2, 3) is supposed to be triggered by low-energy coherent or semicoherent interfaces. During prolonged heating the first TCP phase (most likely sigma) is replaced by another secondary TCP phase (Fig. 2). This precipitation sequence may be caused by various effects. For instance, while growing, TCP phases consume refractory elements, thus leading to depletion of the γ matrix and changes of the lattice constant. This could make the low energy interface less favourable. Alternatively, after longer heating times, slowly diffusing elements that are necessary for the secondary TCP phase have time to accumulate.

Eventually the change of composition leads to γ-dissolution and γ' to become the matrix phase. Finally it leads to achieving equilibrium where the TCP phases are embedded in the new γ' matrix phase and the residues of γ exhibit very irregular shape (Fig. 1b, d, e, 4). The complete phase transformation can be written as:

$$\gamma_{\text{matrix}} + \gamma'_{\text{precipitates}} \rightarrow \gamma'_{\text{matrix}} + \text{TCP} + \gamma_{\text{residual}}.$$

Analysing the microstructures, there is no qualitative change of the phase transformation when Ru is added to the alloy. Ru affects the kinetics of transformation as described in the following subsection.

4.2. TCPs growth kinetic and thermodynamic

Our data shows that addition of Ru to the alloy has the following effects:

1. reduced nuclei density;
2. prolonged incubation time;
3. decreased rate of precipitation;
4. decreased overall content of TCP phases at any time.

Nucleation rate and growth rate of precipitates are the two factors controlling the phenomena above.

Nucleation rate is controlled by diffusion rate and activation energy for nucleation, the latter being a function of driving force and interfacial energy. Growth rate, in turn, is controlled by diffusion rate and driving force.

As reported by Hobbs in [2], the diffusion rate of rhenium is not affected by ruthenium. Thus this factor is considered as the one of lesser significance when it comes to either nucleation or growth stage of precipitation.

The driving force for sigma phase precipitation (and other TCP phases as well) is not influenced by ruthenium, if we believe in the thermodynamic calculations in Fig. 7 and the accuracy of the underlying database. According to simulations, the factor mostly influenced by ruthenium is supposed to be the interface energy between TCP phase and matrix, see Rettig [15, 18]. However, the study on the equilibrium content of TCP phases shows that there is relatively strong divergence between experiments and the Calphad calculations.

We are presently pursuing detailed studies of the interface to check whether any effect of Ru on interfacial energy seems likely or not. The effect of Ru on the equilibrium volume fraction is an indication of a driving force effect, but it is too early to draw final conclusions at this point.

5. Conclusions

1. It is experimentally confirmed that TCP phases precipitate in a sequence. First phases to transform are coherent with the γ/γ' microstructure. In the equilibrium stage TCP phases exhibit semi-coherent or incoherent interfaces with the matrix.
2. The phase transformation occurs according to the scheme:

$$\gamma_{\text{matrix}} + \gamma'_{\text{precipitates}} \rightarrow \gamma'_{\text{matrix}} + \text{TCP} + \gamma_{\text{residual}}.$$

   Ruthenium does not influence the overall phase transformation manner.
3. Ruthenium influences TCP phase precipitation by decrease of nucleation rate and growth rate.

References

[1] M.S.A. Karunaratne, P. Carter, R.C. Reed, Mat. Sci. Eng. **A281**, 229–233 (2000)

[2] R.A. Hobbs, M.S.A Karunaratne, S. Tin, R.C. Reed, C.M.F. Rae, Mat. Sci. Eng. **A460-461**, 587–594 (2007)

[3] A. Heckl, S. Neumeier, M. Göken, R.F. Singer, Mat. Sci. Eng. **A528**, 3435–3444 (2011)

[4] A. Heckl, R. Rettig, R.F. Singer, Met. Mat. Trans A **41A**, 202–211 (2010)

[5] R.A. Hobbs, S. Tin, C.M.F. Rae, R.W. Broomfield, C.J. Humphreys, in *Superalloys 2004* (The Minerals, Metals and Materials Society, Seven Springs, USA, 2004), pp. 819–825

[6] R. Darolia, D. Lahrman , R. Field, in *Superalloys 1988* (The Metallurgical Society, Seven Springs, USA, 1988), pp. 255–264

[7] R.A. Hobbs, L. Zhang, C.M.F. Rae, S. Tin, Met. Mat. Trans. A **39A** 1014–1025 (2008)

[8] C.M.F. Rae, R.C. Reed, Acta Mat. **49**, 4113–4125 (2001)

[9] A.C. Yeh, S. Tin, Met. Mat. Trans. A **37**, 2621–2631 (2006)

[10] M.S.A. Karunaratne, C.M.F. Rae, R.C. Reed, Met. Mat. Trans. A **32A**, 2409–2421 (2001)

[11] M. Simonetti, P. Caron, Mat. Sci. Eng. **A254**, 1–12 (1998)

[12] K. Matuszewski, R. Rettig, M. Rasiński, K.J. Kurzydłowski, R.F. Singer, Adv. Eng. Mat. **16**, 171–175 (2014)

[13] A. Sato, H. Harada, T. Yokokawa, T. Murakumo, Y. Koizumi, T. Kobayashi, Scr. Mat **54**, 1679–1684 (2006)

[14] S. Neumeier, F. Pyczak, M. Göken, in *Superalloys 2008*, (The Minerals, Metals and Materials Society, Seven Springs, USA, 2008), pp. 109-119

[15] R. Rettig, A. Heckl, R.F. Singer, Adv. Mat. Res. **278**, 180–185 (2011)

[16] A.T.W. Kempen, F. Sommer, E.J. Mittemeijer, J. Mater. Sci **37**, 1321–1332 (2002)

[17] D.A. Porter, K.E. Easterling, M.Y. Sherif, *Phase Transformations in Metals and Alloys*, (CRC Press, Boca Raton, Fl, USA, 2009)

[18] R. Rettig, R.F. Singer, in *Superalloys 2012,* (The Minerals, Metals and Materials Society, Seven Springs, USA, 2012), pp. 205–214